Accepted Manuscript

Magnetocaloric effect enhancement driven by intrinsic defects in a $Ni_{45}Co_5Mn_{35}Sn_{15}$ alloy

V. Sánchez-Alarcos, J. López-García, I. Unzueta, J.I. Pérez-Landazábal, V. Recarte, J.J. Beato-López, J.A. García, F. Plazaola, J.A. Rodríguez-Velamazán

PII: S0925-8388(18)33680-6

DOI: 10.1016/j.jallcom.2018.10.016

Reference: JALCOM 47834

To appear in: *Journal of Alloys and Compounds*

Received Date: 20 July 2018

Revised Date: 27 September 2018

Accepted Date: 3 October 2018

Please cite this article as: V. Sánchez-Alarcos, J. López-García, I. Unzueta, J.I. Pérez-Landazábal, V. Recarte, J.J. Beato-López, J.A. García, F. Plazaola, J.A. Rodríguez-Velamazán, Magnetocaloric effect enhancement driven by intrinsic defects in a $Ni_{45}Co_5Mn_{35}Sn_{15}$ alloy, *Journal of Alloys and Compounds* (2018), doi: https://doi.org/10.1016/j.jallcom.2018.10.016.

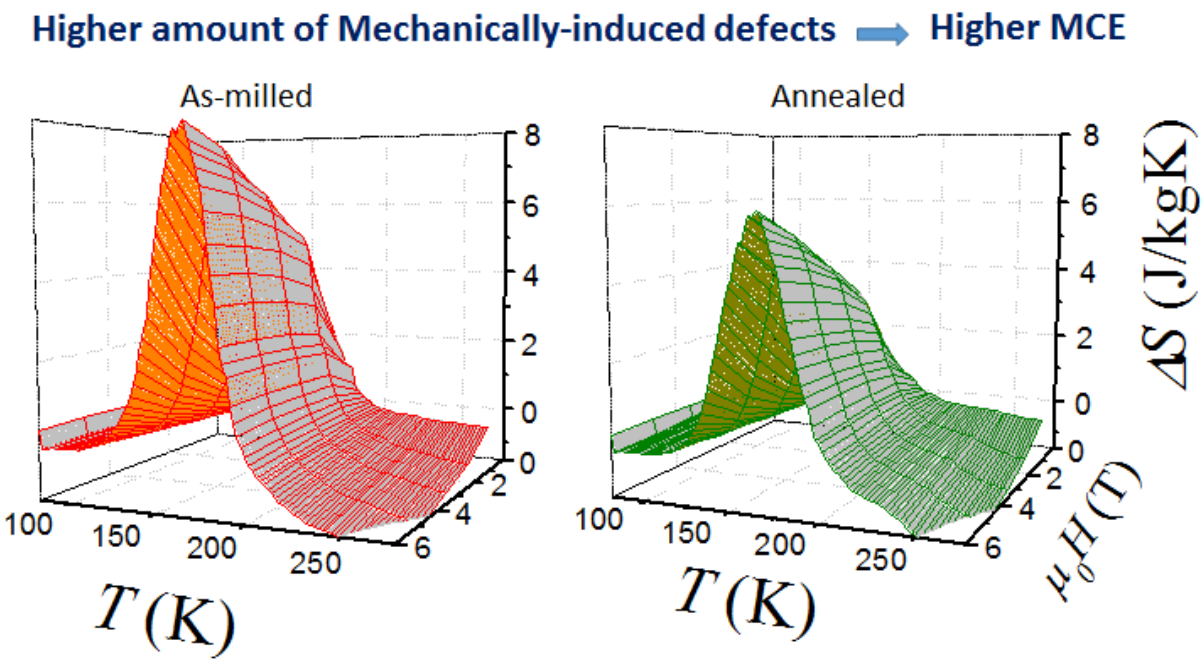

Magnetocaloric effect enhancement driven by intrinsic defects in a $Ni_{45}Co_5Mn_{35}Sn_{15}$ alloy

V. Sánchez-Alarcos[1,2*], J. López-García[1,3], I. Unzueta[4,5], J. I. Pérez-Landazábal[1,2], V. Recarte[1,2], J.J. Beato-López[1,2], J.A. García[5,6], F. Plazaola[4] and J. A. Rodríguez-Velamazán[3]

[1] Departamento Física. Universidad Pública de Navarra, Campus de Arrosadia, 31006 Pamplona, Spain
[2] Institute for Advanced Materials (INAMAT), Universidad Pública de Navarra, Campus de Arrosadía, 31006 Pamplona, Spain
[3] Institut Laue Langevin, 71, Avenue des Martyrs, 38042 Grenoble Cedex, France
[4] Elektrizitate eta Elektronika Saila, Euskal Herriko Unibersitatea UPV/EHU, p.k. 644, 48080 Bilbao, Spain
[5] BC Materials (Basque Centre for Materials, Applications and Nanostructures), 48080 Leioa, Spain
[6] Fisika Aplikatua II Saila, Euskal Herriko Unibersitatea UPV/EHU, p.k. 644, 48080 Bilbao, Spain

*Corresponding author: *Tel.:* +34 948 169582; *Fax.:* +34 948 169565

E-mail address: vicente.sanchez@unavarra.es

Abstract.

The influence of mechanically-induced defects on the magnetostructural properties is analyzed in a Ni-Co-Mn-Sn alloy subjected to soft milling and subsequent annealing treatments. It is found that, opposite to what occurs in Ni-Mn-Sn ternary alloys, the annealing treatment affects the magnetic properties in a different way in martensite and in austenite. In particular, the saturation magnetization significantly increases in martensite after annealing whereas just a very slight variation is observed in austenite. This leads to the interesting fact that the presence of microstructural defects, far for worsening, makes the magnetocaloric effect to be higher in the as-milled state than after annealing. This behavior is explained as the result of the combination of the effect of defects on the Mn-Mn distance, the effect of Co on the magnetic exchange coupling between Mn atoms, and the effect of defects on the vibrational entropy change at the martensitic transformation.

Keywords: Ni-Mn-Sn-Co, magnetocaloric effect, defects, vibrational entropy

1. INTRODUCTION

Ni-Mn-based metamagnetic shape memory alloys are being widely studied during the last decade because of the unique multifunctional features they show as a result of the interplay between a structural transformation and a complex magnetic ordering. Due to the strong dependence of the magnetic exchange interactions on the Mn-Mn distances [1-3], the change in the interatomic distances caused by the occurrence of a thermoelastic martensitic transformation (MT) in some of these alloys results in a large magnetization change (ΔM) at the transformation temperature that favors the induction of the structural transformation by an applied magnetic field [4-7]. Such magnetic induction of the MT, and the different features of the different structural phases (austenite and martensite), give rise to interesting properties such as the magnetic shape memory effect, large magnetoresistance or giant inverse magnetocaloric effect, that make these alloys very attractive for practical applications in sensing and magnetic refrigeration [8-18].

The most promising alloys for magnetocaloric applications are those alloys in the Ni-Mn-X (X=In, Sn, and Sb) systems in which the MT takes place between a ferromagnetic austenite and a weaker-magnetic martensite. The MT characteristics and the magnetic properties of these alloys depend on composition, atomic order and, to a lesser extent, on microstructure. The compositional dependence has been widely studied, being the complete phase diagrams of the appearing structural and magnetic phases well stablished [19-22]. Atomic order has been also systematically studied. In Ni-Mn-In and Ni-Mn-In-Co alloys it has been shown that the magnetostructural properties can be properly tuned varying the long-range atomic order, which can be easily controlled by means of thermal treatments [23-25]. In Ni-Mn-Sn and Ni-Mn-Sb alloys, in turn, the $L2_1$ structure is highly stable and the atomic order is then hardly modifiable by means of conventional thermal treatments [26]. In these alloys, the modification of the microstructural parameters (grain size, defects, internal stresses…) is the only way to modify the functional properties for a selected alloy composition. Mechanical milling and subsequent annealing treatments are one of the simplest and most used method to modify the

microstructure. Typically, the grain size reduction and the presence of defects and internal stresses induced by milling degrade the MT and the magnetic properties, which can be then partially restored upon microstructural recovery processes brought by subsequent annealing [27-32]. In this respect, by comparing a Ni-Mn-Sn alloy in both the as-milled and the annealed states, we have recently shown that, even though no appreciable long-range atomic disorder was induced by milling, the saturation magnetization of both martensitic and austenitic phases are considerably higher after annealing, due to the reduction of the density of the anti-phase boundaries (linked to dislocations) which promote the antiferromagnetic coupling between Mn moments [32]. A similar magnetic deterioration at anti-phase boundaries was indeed evaluated in Ni-Mn-Al-Ga alloys by electron holography, and explained as a consequence of a local atomic disordering in the boundary region [33].

The addition of Cobalt has been shown to enhance the magnetism of the austenite and to hinder ferromagnetic ordering in martensite in Ni-Mn-X alloys, thus leading to an increase of ΔM and therefore to larger magnetically-induced shifts of the MT temperature and higher associated magnetocaloric effects [4, 34-38]. In particular, in Ni-Mn-Sn alloys it has been also shown that the magnetic coupling between the Mn moments on the 4a (Mn sublattice) and 4b sites (Sn sublattice) of the austenitic cubic structure changes from being antiferromagnetic to ferromagnetic as a consequence of the substitution of Ni by Co [37] (the magnetic coupling between Mn atoms on the 4a sites is ferromagnetic both in the ternary and the quaternary alloys). In this regard, it could be thought that the influence of the presence of anti-phase boundaries (and any other microstructural defect resulting in local atomic disordering) on the magnetic properties will be different in the quaternary Co-doped alloys to that in the ternary ones. In this sense, the effect of mechanically-induced defects on the magnetostructural properties, and in particular on the magnetocaloric effect, is analyzed on a quaternary Ni-Co-Mn-Sn alloy subjected to soft milling and subsequent annealing. It is found that the presence of microstructural defects, far for worsening, can make the magnetocaloric effect to be higher in the as-milled state than after subsequent annealing. This unusual beneficial presence of defects

is explained as the result of the combination of the effect of defects on the Mn-Mn distance, the effect Co on the magnetic exchange coupling between Mn atoms, and the effect of defects on the vibrational entropy change at the martensitic transformation.

2. EXPERIMENTAL

A $Ni_{45}Co_5Mn_{35}Sn_{15}$ alloy was prepared from high purity elements by arc melting under protective Ar atmosphere. The as-cast ingot was homogenized at 1173 K during 24h and then slowly cooled to RT. The composition was analyzed by EDS in a Jeol JSM-5610LV Scanning Electron Microscope (SEM). In order to induce defects, the alloy was subjected to hand milling in an agate mortar until reaching a uniform particle-size distribution. The mean particle size of the powder, estimated from SEM images, was 60 ± 20 μm. A part of the obtained powder was then subjected to a 5 minutes annealing at 673 K in order to remove some of the defects induced by milling. In previous works, such annealing treatment has been shown (from Mössbauer spectroscopy and XR diffraction measurements) to cause a significant microstructural evolution in milled ternary Ni-Mn-Sn alloys [32, 39]. The microstructural states obtained in the as-milled and the annealed samples were then analyzed and compared: the martensitic transformations were characterized by differential scanning calorimetry (Q-100 DSC, TA Instruments), on heating ramps performed from 140 K up to 300 K at 10 K/min; the magnetic properties (low and high field magnetization) by SQUID magnetometry (QD MPMS XL-7); and the crystallographic and magnetic structures were determined from powder neutron diffraction measurements performed on the D1B diffractometer, at the Institute Laue-Langevin (Grenoble, France), using a neutron wavelength of 1.28 Å. The structures were refined by the Rietveld method using the FullProf package programs [40].

3. RESULTS AND DISCUSSION

Figure 1 shows the temperature dependence of the magnetization in the as-milled and annealed samples under (a) $7.95 \cdot 10^3$ A/m (100 Oe) and (b) $4.77 \cdot 10^6$ A/m (60 kOe) applied magnetic fields. The sequences of magnetostructural transformations can be clearly determined from the low-field *M(T)* curves: in both samples, the high temperature paramagnetic austenite becomes ferromagnetic around 360 K and a subsequent magnetization jump takes place around 180 K linked to the martensitic transformation to a weaker-magnetic martensite. The occurrence of such martensitic transformation is confirmed from the appearance of endothermic peaks (see inset) associated to the reverse MT on the heating curves in calorimetric measurements. The transformation temperatures and the magnetization change at the MT obtained from the different *M(T)* curves are summarized in Table 1 along with the entropy change at the MT, ΔS, estimated from the DSC thermograms. As it occurred in ternary Ni-Mn-Sn alloys [32], neither the Curie temperature, T_C^a, nor the MT temperature, T_M, seem to evolve substantially with the annealing treatment. Taking into account the high sensibility of these transition temperatures to long-range atomic order [41], the absence of evolution suggests a scarce effect of annealing on atomic order, as it could be indeed expected given the high stability of the $L2_1$ structure in the Ni-Mn-Sn system [26]. With respect to the entropy change it is worth noting that obtained value is higher in the as-milled sample in spite of ΔS typically increases as a consequence of the microstructural recovery processes brought by annealing (as in fact occurs in ternary Ni-Mn-Sn alloys [39]). This point will we analyzed later in detail. On the other hand, the thermal hysteresis linked to the MT is also practically unaffected by annealing (in fact, it is slightly larger in the annealed sample). As shown in Figure 1b, the MT shifts toward lower temperatures under the application of a $4.77 \cdot 10^6$ A/m magnetic field, being the shift (with respect to T_M obtained at $7.95 \cdot 10^3$ A/m) almost the same in both as-milled and annealed samples. On the contrary, the magnetization change at the MT, ΔM, is definitively affected by annealing, being ΔM quite lower in the annealed sample.

The effect of annealing on the saturation magnetization, M_S, is illustrated in Figure 2, where the magnetic-field dependence of magnetization is shown for both phases in both as-milled and

annealed states. In all cases, the magnetization shows an initial abrupt increase and a subsequent trend to saturation, typical of a ferromagnetic behavior. Interestingly, the annealing treatment affects the magnetization in a different way in martensite and in austenite. In particular, the saturation magnetization significantly increases in martensite after annealing ($\Delta M_S^{mart}/ M_S^{mart}$ ~ 28%) whereas a very slight variation ($\Delta M_S^{aust}/ M_S^{aust}$ ~ 3%) is observed in austenite. This behavior is quite surprising as long as it is opposite to that found in similarly-milled ternary Ni-Mn-Sn alloys, for which the high-field magnetization increase linked to annealing is larger in austenite and in martensite [32].

In order to ascertain the origin of the different evolution of the saturation magnetization in martensite and austenite upon annealing, neutron diffraction measurements were performed. Figure 3 shows the obtained diffractograms together with the Rietveld refinement of the diffraction patterns. The nuclear structures have been first refined from diffractograms obtained at 400 K in paramagnetic austenite, which allowed a more accurate determination of the site occupancy, and then a combined nuclear and magnetic refinement has been performed for ferromagnetic austenite at 300 K and ferromagnetic martensite at 10K. The structural and magnetic parameters obtained after Rietveld refinement are shown in Table 2. Both in martensite and in austenite, the crystallographic structure is the same before and after annealing. The austenitic phases show the typical cubic $L2_1$ structure (space group $Fm\bar{3}m$) with almost the same lattice parameter. Some of the intensity peaks indexed according to the associated Bragg reflections are shown in the diffractograms. In particular, the (111), (200) and (220) superstructure reflections, linked to the $L2_1$, B2 and A2 type of ordering, respectively [26, 42], are clearly distinguished at low angles. As expected, no significant variation of the atomic order is observed, in agreement with the null evolution of the structural and magnetic transition temperatures. Likewise, the martensitic structure is the same in both samples; a 3M modulated monoclinic structure (space group *P2/m*) with similar lattice parameters, no trace of austenitic phase being observed at all at 10 K. With respect to the refined magnetic structure (a collinear magnetic structure, in all cases), it is first worth noting that the magnetic moments of Mn atoms

are all positive in austenite, thus confirming the ferromagnetic coupling between Mn atoms, even between those in the 4a and 4b sites. On the contrary, negatives moments are obtained in martensite for Mn atoms in those sites resulting from the monoclinic distortion of the 4b sites (as expected due to the weakening of the exchange interactions as a consequence of the abrupt change in the Mn–Mn interatomic distances upon the MT [43]). Interestingly, the net magnetic moments in austenite are unaffected by annealing whereas a significant influence of annealing is observed on the magnetic moments in martensite, where a marked decrease in the negative antiferromagnetic contribution is observed.

Since neither crystallographic structure nor lattice parameters nor long-range atomic order evolve upon annealing, the observed evolution of the saturation magnetization and the magnetic moments in martensite must be purely attributable to a microstructural relaxation, just as it occurs in a similarly-milled ternary Ni-Mn-Sn alloy [32]. In that case, the increase of the saturation magnetization of austenite and martensite after annealing was ascribed to a reduction of the density of anti-phase boundaries as a result of the annihilation of superlattice dislocations. In the cubic phase of the ternary Ni-Mn-Sn alloys, the magnetic coupling between Mn atoms in the 4a sites is ferromagnetic whereas it is antiferromagnetic between Mn atoms in the 4a and 4b sites [32]. Hence, the magnetic coupling between Mn atoms may change from ferromagnetic to antiferromagnetic across linear or planar defects, thus leading to a decrease in the net magnetic moment. In the austenitic phase of the quaternary alloy, in turn, the presence of Co on the Ni sites makes the Mn atoms at the 4a and 4b sites to couple ferromagnetically, and therefore the magnetic coupling between Mn atoms (whether nearest or next-nearest neighbors) will be always ferromagnetic, irrespectively of the presence of defects. Therefore, assuming that a similar annihilation process occurs on annealing the quaternary alloy, the almost null evolution of the saturation magnetization of austenite can be explained as a direct consequence of the ferromagnetic coupling between Mn atoms. With respect to the martensitic phase, the change in the interatomic distances upon the martensitic transformation makes the Mn atoms in the martensitic structure to couple antiferromagnetically or ferromagnetically depending on whether

they are nearest or next-nearest neighbors, respectively, both in the ternary and the quaternary alloys. Therefore, the change of the Mn-Mn distance associated to the presence of defects (or even to internal stresses) may explain the lower antiferromagnetic contribution in the annealed sample, where the amount of defects is presumably lower than in the as-milled one.

The effect of defects on the magnetic properties can be qualitatively estimated from the fitting of the field-dependence of the magnetization to the classical law of approach to saturation for magnetization

$$M = M_S\left(1-\frac{a}{H}-\frac{b}{H^2}\right)+\chi H \qquad (1)$$

where H is the applied field, M_S the saturation magnetization, χ the field independent susceptibility and a and b are coefficients related to magnetic and structural properties of the sample [44-46]. In particular, the parameter a depends on the stresses field created by dislocations and non-magnetic inclusions and it can be approximated to $a \approx 4\pi\rho M_S P_{eff}$, where ρ is the density of the material and P_{eff} is the effective fraction of porosity and non-magnetic inclusions [47]. From the fitting of the magnetization curves in martensite at 10 K to the law of approach to saturation (Figure 2b) P_{eff} values of 0.021 and 0.014 are obtained for the as-milled and annealed samples, respectively. The higher value of effective fraction of non-magnetic inclusions in the as milled sample points out that the density of dislocations where the ferromagnetic coupling is lost by the local atomic disordering is higher in the as-milled sample than in the annealed one, in agreement with the expected reduction of defects upon heating treatment.

The magnetically-induced shift of T_M is directly related to ΔM through the Clausius-Clapeyron equation

$$\frac{dT_M}{dH} = -\mu_0\frac{\Delta M}{\Delta S} \qquad (2)$$

(where H is the applied magnetic field). The observed effect of annealing on the magnetic moments, and in particular on ΔM, suggests a possible influence of the mechanically-induced defects on the magnetic induction of the MT and therefore on the magnetocaloric effect (MCE).

The effect of magnetic field on the MT temperature has been analyzed from the temperature dependence of magnetization under different applied magnetic fields. Figure 4a shows the *M(T)* curves obtained on heating under applied magnetic fields ranging from $7.95 \cdot 10^3$ A/m to $4.77 \cdot 10^6$ A/m around the martensitic transformation of the as-milled and the annealed samples. As expected, in both cases the magnetization jump associated to the MT occurs at lower temperatures on increasing the magnetic field, because of the magnetic stabilization of the austenite. The shift of T_M (determined from the peaks of the derivative curve of magnetization measurements) is shown in Figure 4b as a function of the applied field. The transformation temperatures linearly decrease with the increasing applied field, being the slope the same in both samples, $dT_M/dH \approx 6.3 \cdot 10^{-6}$ K/(A/m) (0.5 K/kOe). It is worth noting that this slope is in agreement with the dT_M/dH values calculated by substituting into Equation 1 the values of ΔM and ΔS shown in Table 1.

The MCE, which can be defined as the entropy change in isothermal conditions, ΔS_{iso}, has been calculated from the ZFC magnetization measurements shown in Figure 4a using the expression

$$\Delta S_{iso} = S(T,H) - S(T,0) = \int_0^H \left(\frac{\partial M}{\partial T}\right)_H dH \qquad (3)$$

The numerical integration of $\partial M/\partial T$ from a set of magnetization versus temperature spectra at different constant values of applied field $M(T)_H$ is the correct procedure [48]. The obtained ΔS_{iso} values are shown in Figure 5 as a function of temperature and applied magnetic field. In both cases, a positive peak (inverse MCE) is observed linked to the magnetostructural transformation at T_M^{rev} and the maximum MCE values increase with the increasing magnetic field. In particular, the maximum values, obtained under $4.77 \cdot 10^6$ A/m, are $\Delta S_{iso}^{Mill} \approx 8$ J/kgK and $\Delta S_{iso}^{Ann} \approx 6$ J/kgK for the milled and annealed samples, respectively. These values are much lower than the higher

values obtained in Ni-Co-Mn-Sn alloys (around $\Delta S_{iso} \approx 32$ J/kgK [49]), but comparable or even greater than those obtained in the Ni-Mn-Sn system [11, 17, 27]. In order to better compare the influence of annealing on the magnitude of the MCE, the ΔS_{iso} values obtained in both samples are plotted together as a function of temperature in Figure 6. It can be seen that the magnetocaloric effect is considerably higher in the as-milled sample than in the annealed one. Interestingly, this result suggest that the presence of defects, far for worsening, may be beneficial for MCE in metamagnetic Heusler alloys.

In this alloys the magnetically-induced entropy change is linked to the magnetic induction of the MT. In both, the as-milled and annealed samples, a similar transformed fraction is induced since the shift of the MT temperature and the width of the MT temperature range is nearly the same. Therefore, the higher ΔS_{iso} obtained in the as-milled sample must a consequence of its higher intrinsic MT entropy change (see table 1). The entropy change linked to the reverse MT (represents the maximum attainable ΔS_{iso}) can be considered as the sum of a vibrational $\Delta S_{vib}^{(+)}$ (positive) and a magnetic $\Delta S_{mag}^{(-)}$ (negative) term, in such a way that $\Delta S \approx \Delta S_{vib}^{(+)} + \Delta S_{mag}^{(-)}$ must be positive [50]. Since $\Delta S_{mag}^{(-)}$ (directly related to ΔM [42]) is higher in the as-milled sample, a lower total ΔS should be expected. Nevertheless, ΔS is actually higher indicating that the vibrational contribution ΔS_{vib} must be considerably higher in the as-milled sample than in the treated one. Taking into account that the crystallographic structures are exactly the same in both samples, the decrease of the entropy change in the treated sample should be attributable to the decrease in the concentration of mechanically-induced defects upon annealing. Assuming that in general the presence of defects increase the entropy of the alloy independently of the crystallographic structure (phase), the increase of the vibrational entropy change ΔS_{vib} is a consequence of the much stronger influence of the induced defects on the vibrational entropy of the austenite than on the vibration entropy of the martensite (opposite to the above mentioned higher influence of defects on the magnetism of the martensitic phase). Although the influence of defects (point defects, dislocations and anti-phase boundaries) in the vibrational properties of some metals has been analyzed in several theoretical studies [51-53], up to our knowledge this is the first indirect evidence of the effect of defects on the vibrational entropy change at the

martensitic transformation. In any case, further works on the analysis of the type and concentration of defects should be need in order to quantitatively correlate defects and magnetically-induced entropy change.

3. SUMMARY AND CONCLUSSIONS

The influence of mechanically-induced defects on the magnetostructural properties is analyzed in a Ni-Co-Mn-Sn alloy. It is found that the mechanically-induced defects, far for worsening, improve the magnetocaloric response. This is due to two main features; first, the different exchange coupling between nearest-neighbors Mn atoms in the austenitic and in the martensitic structures makes the magnetization change at the martensitic transformation to be increased as a result of the presence of defects. Second, the mechanically-induced defects increase the vibrational entropy change at the transformation, thus leading to a higher total entropy change and, therefore, to a higher attainable magnetocaloric effect. Given the difficulty to modify the atomic order in the Ni-Mn-Sn system by means of conventional thermal treatments, the presented results show that, once fixed the composition, the induction of microstructural defects can be an effective way to enhance the multifunctional properties of these alloys.

This work has been carried out with the financial support of the Spanish "Ministerio de Economía y Competitividad" (Projects number MAT2015-65165-C2-R) and of the Basque Government (Grant No. IT-1005-16). We also acknowledge ILL and SpINS for beam time allocation: experiments 5-24-591 (http://dx.doi.org/10.5291/ILL-DATA.5-24-591) and CRG-2352. J. López-García acknowledges ILL for his Ph. D. contract and I. Unzueta also wants to thank the Basque Government Grant No. PRE-2014-1-214.

References

[1] E. Sasioglu, L.M. Sandratskii, P. Bruno, Phys. Rev. B 70 (2004) 024427.

[2] E. Sasioglu, L. M. Sandratskii, and P. Bruno, Phys. Rev. B 77 (2008) 064417.

[3] V. D Buchelnikov, P. Entel, S. V Taskaev, V. V. Sokolovskiy, A. Hucht, M. Ogura, H. Akai, M. E. Gruner, and S.K. Nayak, Phys. Rev. B 78 (2008) 184427.

[4] R. Kainuma, Y. Imano, W. Ito, Y. Sutou, H. Morito, S. Okamoto, K. Kitakami. A. Oikawa, O. Fujita, T. Kanomata, and K. Ishida, Nature 439 (2006) 957.

[5] K. Koyama, K. Watanabe, T. Kanomata, R. Kainuma, K. Oikawa, and K. Ishida, Appl. Phys. Lett. 88 (2006) 132505.

[6] K. Oikawa, W. Ito, Y. Imano, Y. Sutou, R. Kainuma, K. Ishida, S. Okamoto, O. Kitakami, and T. Kanomata, Appl. Phys. Lett. 88 (2006)122507.

[7] M. Acet, Ll. Mañosa, and A. Planes, in: K.H.J. Buschow (Ed), Handbook of magnetic materials Vol.19, Elsevier, Amsterdam, 2011, pp. 231-289.

[8] R. Kainuma, W. Ito, R. Y. Umetsu, and V. V. Khovaylo, Mater. Sci. Forum 684 (2011) 139.

[9] S. Y. Yu, Z. H. Liu, G. D. Liu, J. L. Chen, Z. X. Cao, G. H. Gu, B. Zhang, and X. X. Zhang, Appl. Phys. Lett. 89 (2006) 162503.

[10] V. K. Sharma, M. K. Chattopadhyay, K. H. B. Shaeb, A. Chouhan, and S. B. Roy, Appl. Phys. Lett. 89 (2006) 222509.

[11] T. Krenke, E. Duman, M. Acet, E. F. Wassermann, X. Moya, Ll. Mañosa, and A. Planes, Nat. Mat. 4 (2005) 450.

[12] T. Krenke, E. Duman, M. Acet, E. F. Wassermann, X. Moya, Ll. Mañosa, A. Planes, E. Suard, and B. Ouladdiaf, Phys. Rev. B 75 (2007) 104414.

[13] M. Khan, A. Pathak, M. R. Paudel, I. Dubenko, S. Sadler, N. Ali, J. Magn. Magn. Mater. 320 (2008) L21-L25.

[14] A. Planes, Ll. Mañosa, and M. Acet, J. Phys.: Condens. Matter. 21 (2009) 233201.

[15] J. Liu, T. Gottschall, K. P. Skokov, J. K. Moore, and O. Gutfleisch, Nature Mater. 11 (2012) 620.

[16] I. Dubenko, et. al., Magnetic, Magnetocaloric, Magnetotransport, and Magneto-optical Properties of Ni-Mn-In-Based Heusler Alloys: Bulk, Ribbons, and Microwires, Chapter II in hardcover book: Novel Functional Magnetic Materials: Fundamentals and Applications (ed. A. Zhukov), Springer, Series in Materials Science 231, (2016) pp.41-83.

[17] A. Aryal, A. Quetz, S. Pandey, I. Dubenko, S. Stadler, and N. Ali, J. Alloy. Comp. 717 (2017) 254.

[18] S. Pandey, A. Quetz, A. Aryal, I. Dubenko, D. Mazumdar, S. Stadler, and N. Ali, Magnetochemistry 3 (2017) 3, 3

[19] Y. Sutou, Y. Imano, N. Koeda, T. Omori, R. Kainuma, K. Ishida, and K. Oikawa, Appl. Phys. Lett. 85 (2004) 4358.

[20] T. Krenke, M. Acet, E. F. Wassermann, X. Moyà, Ll. Mañosa, and A. Planes, Phys. Rev. B 72 (2005) 014412.

[21] T. Krenke, M. Acet, E. F. Wassermann, X. Moyà, Ll. Mañosa, and A. Planes, Phys. Rev. B 73 (2006) 174413.

[22] M. Khan, I. Dubenko, S. Stadler, and N. Ali, J. Phys.: Condens. Matter. 20 (2008) 235204.

[23] V. Recarte, J. I. Pérez-Landazábal, V. Sánchez-Alarcos, and J. A. Rodríguez-Velamazán, Acta Mater. 60 (2012) 1937.

[24] V. Recarte, J. I. Pérez-Landazábal, and V. Sánchez-Alarcos, J. Alloy. Comp. 536 (2012) S308.

[25] V. Sánchez-Alarcos, V. Recarte. J. I. Pérez-Landazábal, E. Cesari, and J. A. Rodríguez-Velamazán, Entropy 16 (2014) 2756.

[26] V. Sánchez-Alarcos, J. I. Pérez-Landazábal, V. Recarte, I. Lucia, J. Vélez, and J. A. Rodríguez-Velamazán, Acta Mater. 61 (2013) 4676.

[27] A. L. Alves, E. C. Passamani, V. P. Nascimento, A. Y. Takeuchi, and C. J. Larica, J. Phys. D: Appl. Phys. 43 (2010) 345001.

[28] E. C. Passamani, V. P. Nascimento, C. J. Larica, A. Y. Takeuchi, A. L. Alves, J. R. Proveti, M. C. Pereira, and J. D. Fabris, J. Alloy. Comp. 509 (2011) 7826.

[29] A. Ghotbi Varzaneh, P. Kameli, V. R. Zahedi, F. Karimzadeh, and H. Salamati, Met. Mater. Int. 4 (2015) 758.

[30] P. Czaja, J. Przewoznik, M. Fitta, M. Balanda, A. Chrobak, B. Kania, P. Zackiewicz, A. Wójcik, M. Szlezynger, and W. Maziarz, J. Magn. Magn. Mater. 401 (2016) 223.

[31] X. Wang, F. Sun, J. Wang, Q. Yu, Y. Wu, H. Hua, and C. Jiang, J. Alloy. Comp. 691 (2017) 215.

[32] I. Unzueta, J. Lopez-García, V. Sánchez-Alarcos, V. Recarte, J. I. Pérez-Landazábal, J. A.Rodríguez-Velamazán, J. S. Garitaonandia, J. A. García, and F. Plazaola, Appl. Phys. Lett. 110 (2017) 181908.

[33] Y. Murakami, K. Yanagisawa, K. Niitsu, H. S. Park, T. Matsuda, R. Kainuma, D. Shindo, and A. Tonomura, Acta Mater. 61 (2013) 2095.

[34] R. Kainuma, Y. Imano, W. Ito, H. Morito, Y. Sutou, K. Oikawa, A. Fujita, K. Ishida, S. Okamoto, O. Kitakami, and T. Kanomata, Appl. Phys. Lett. 88 (2006) 192513.

[35] A. K Nayak, K.G. Suresh, and A.K. Nigam, J. Phys. D: Appl. Phys. 42 (2009) 035009.

[36] L. Huang, D. Y. Cong, H. L. Suo, and Y. D. Wang, Appl. Phys. Lett. 104 (2014)132407.

[37] R. Y. Umetsu, A. Sheikh, W. Ito, B. Ouladdiaf, K. R. A. Ziebeck, T. Kanomata, and R. Kainuma, Appl. Phys. Lett. 98 (2011) 042507.

[38] S. Pandey, A. U. Saleheen, A. Quetz, J-H Chen, A. Aryal, I. Dubenko, P. W. Adams, S. Stadler, N. Ali, MRS commun. 7 (2017) 885.

[39] J. López-García, I. Unzueta, V. Sánchez-Alarcos, V. Recarte, J. I. Pérez-Landazábal, J. A. Rodríguez-Velamazán, J. A. García, and F. Plazaola, Intermetallics 94 (2018) 133.

[40] J. Rodríguez-Carvajal, Physica B 192 (1993) 55.

[41] V. Sánchez-Alarcos, V. Recarte. J. I. Pérez-Landazábal, C. Gómez-Polo, and J.A. Rodríguez-Velamazán, Acta Mater. 60 (2012) 3168.

[42] V. Sánchez-Alarcos, J. I. Pérez-Landazábal, V. Recarte, Mater. Sci. Forum 686 (2011) 85.

[43] V. V. Khovaylo, T. Kanomata, T. Tanaka, M. Nakashima, Y. Amako, R. Kainuma R, R. Y. Umetsu, H. Morito, and H. Miki, Phys. Rev. B 80 (2009) 144409.

[44] S. Chikazumi, Physics of Magnetism, Willey, 1964.

[45] E.J. Schlomann, J. Appl. Phys. 38 (1967) 5027.

[46] H. Zhang, D. Zeng, Z. Liu, J. Magn. Magn Mater. 322 (2010) 2375.

[47] G.F. Donne, J.A. Weiss, A.A. Gary, J. Appl. Phys. 61 (1987) 3862.

[48] L. Tocado, E. Palacios, and R. Burriel, J. Appl. Phys. 105 (2009) 093918.

[49] L. Huang, D. Y. Cong, L. Ma, Z. H. Nie, M. G. Wang, Z. L Wang, H. L. Suo, Y. Ren, and Y. D. Wang, J. Alloy. Comp. 647 (2015) 1081.

[49] V. Recarte, J. I. Pérez-Landazábal, V. Sánchez-Alarcos, V. Zablotskii, E. Cesari, and S. Kustov, Acta Mater. 60 (2012) 3168.

[50] M. Forsblom, N. Sandberg, and G. Grimvall, Phil. Mag. 84 (2004) 521.

[1] P. C. Shuck, J. Marian, J. B. Adams, and B. Sadigh, Phil. Mag. 89 (2009) 2861.

[52] V. R. Manga, S. L. Shang, W. Y. Wang, Y. Wang, J. Liang, V. H. Crespi, and Z. K. Liu, Acta Mater. 82 (2015) 287.

Figure captions

FIG. 1: Temperature dependence of magnetization of the as-milled and annealed samples under (a) $7.95 \cdot 10^3$ A/m and (b) $4.77 \cdot 10^6$ A/m applied magnetic field. Inset in Fig.1a: detail of the heating curve of the DSC thermogram.

FIG. 2: (a) Magnetization in the austenitic (at 225 K) and martensitic (at 10 K) phases of the as-milled and annealed samples, as a function of the applied magnetic field. (b) Detail of the fitting of the magnetization curves in martensite at 10 K to the law of approach to saturation

FIG. 3: Measured neutron diffraction pattern (dots), calculated profile (full line) and difference between the measured and calculated profiles (dashed line) for the as-milled and treated samples alloy at (a) 300K (austenite) and (b) 10 K (martensite).

FIG. 4: (a) ZFC *M(T)* curves on heating under different applied fields ranging from $7.95 \cdot 10^3$ A/m up to $4.77 \cdot 10^6$ A/m in the as-milled and annealed samples. (b) Shift of the transformation temperature as a function of the applied magnetic field.

FIG. 5: Isothermal magnetically-induced entropy change as a function of temperature and applied magnetic field for (a) as-milled sample and (b) annealed sample.

FIG. 6: Isothermal magnetically-induced entropy change under $4.77 \cdot 10^6$ A/m applied magnetic field as a function of temperature for the as-milled and annealed samples.

Table captions

Table. 1: Temperature of the reverse martensitic transformation (T_M^{rev}) at $7.95 \cdot 10^3$ A/m and $4.77 \cdot 10^6$ A/m, Curie temperature of the austenite (T_C^a) and entropy change at the MT (ΔS) for the as-milled and annealed samples.

Table. 2: Structural and magnetic parameters obtained from Rietveld refinement of the neutron diffraction patterns at 300 K (austenite) and 10 K (martensite) in the as-milled and annealed samples. *The magnetic moments of Ni and Co in site 8c are assumed to be 0.2 μB and 1.0 μB respectively

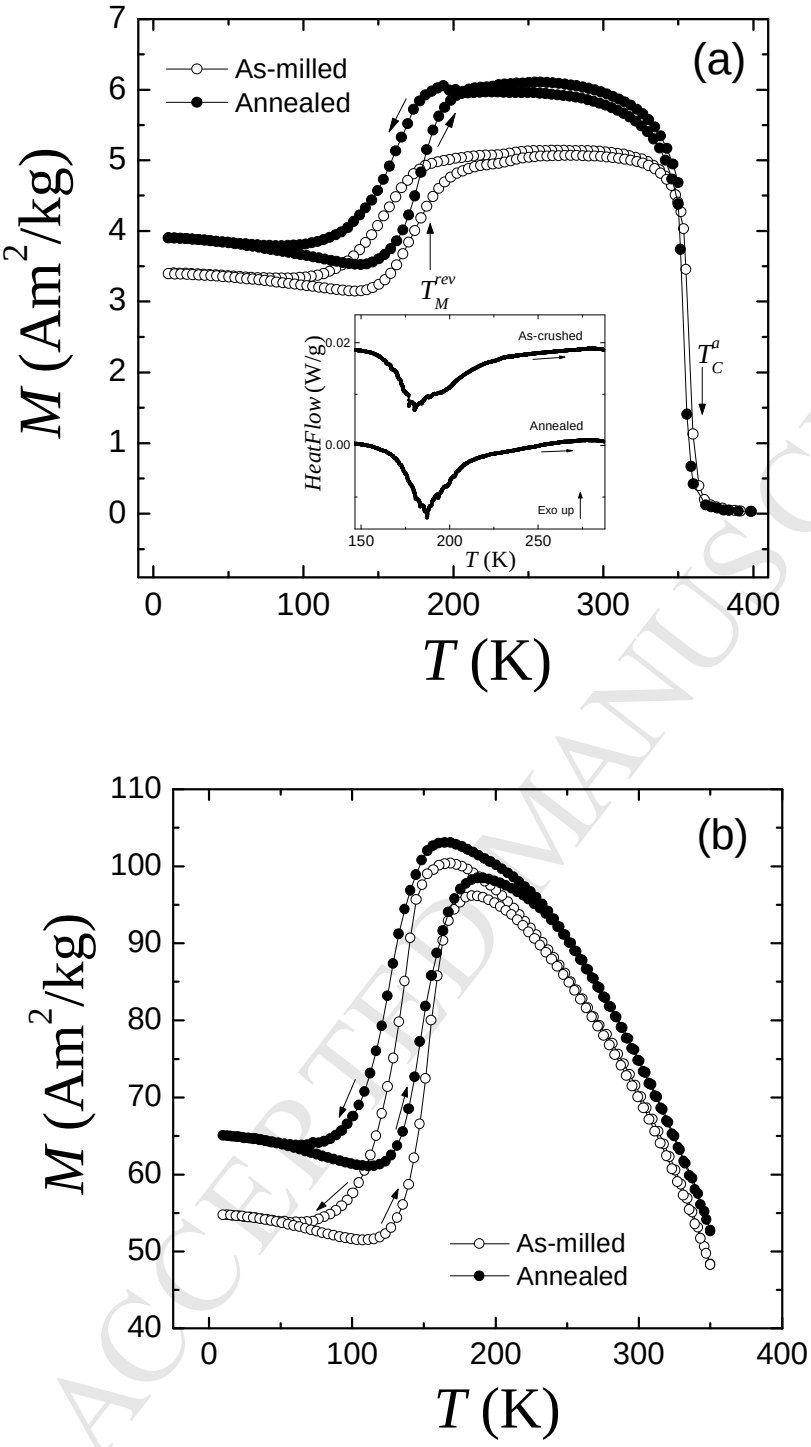

Fig.1

Sánchez-Alarcos et al.

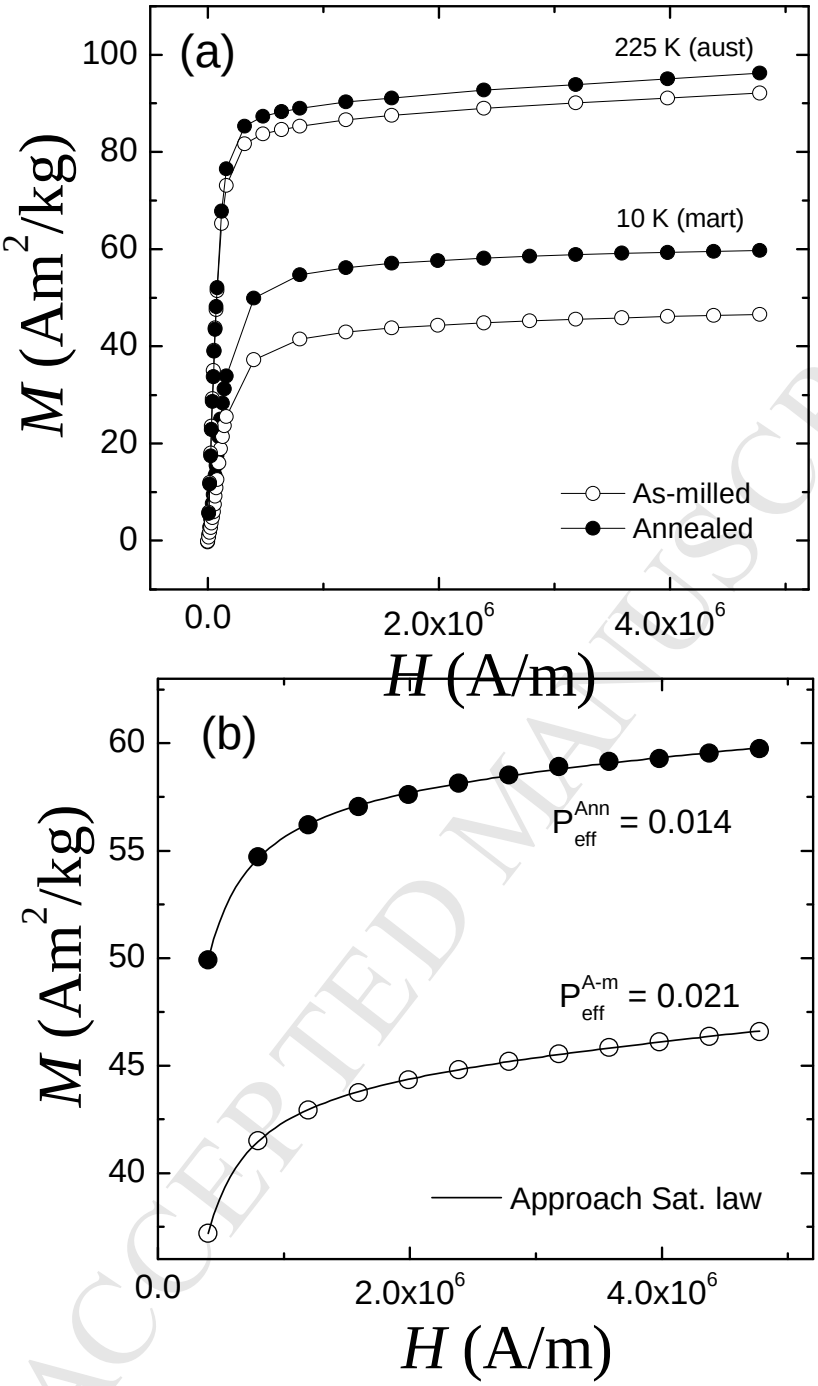

Fig.2

Sánchez-Alarcos et al.

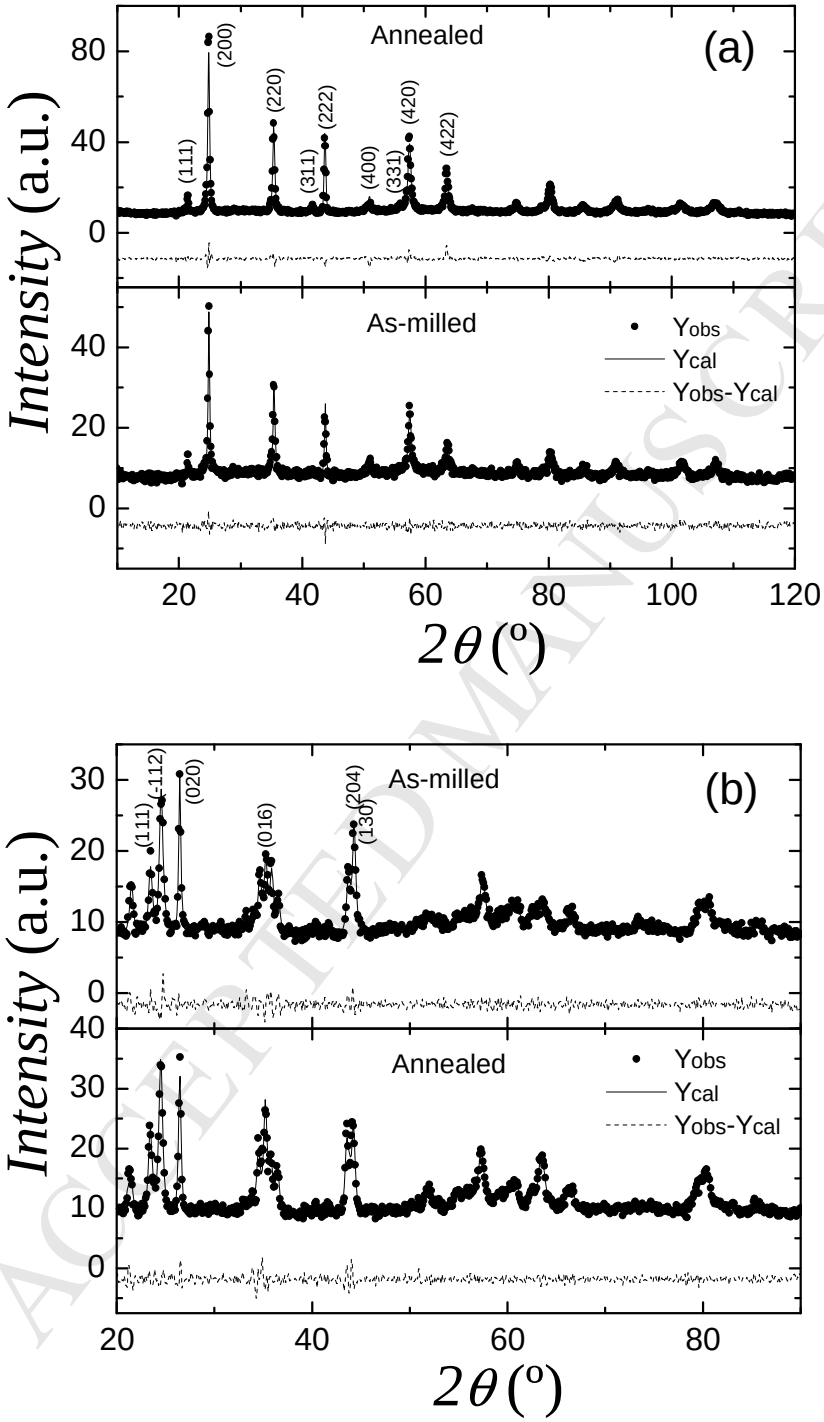

Fig.3

Sánchez-Alarcos et al.

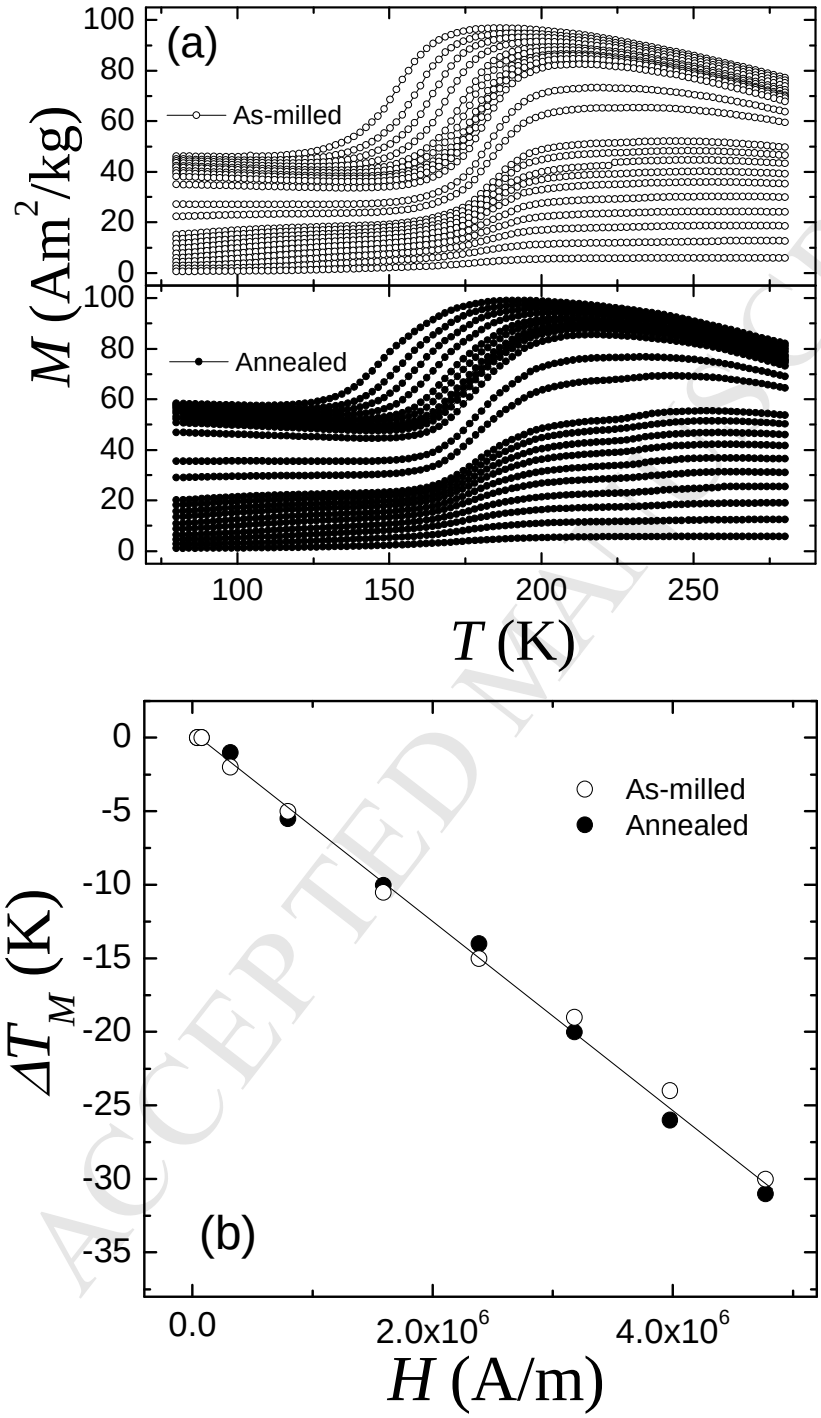

Fig.4

Sánchez-Alarcos et al.

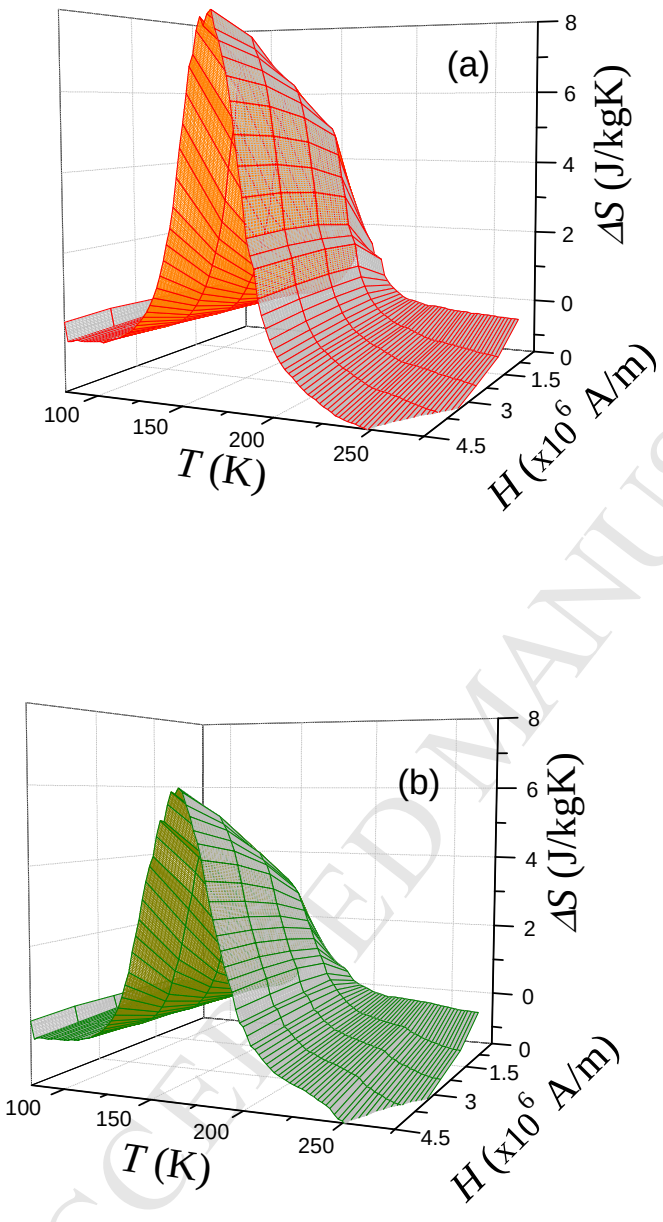

Fig.5

Sánchez-Alarcos et al.

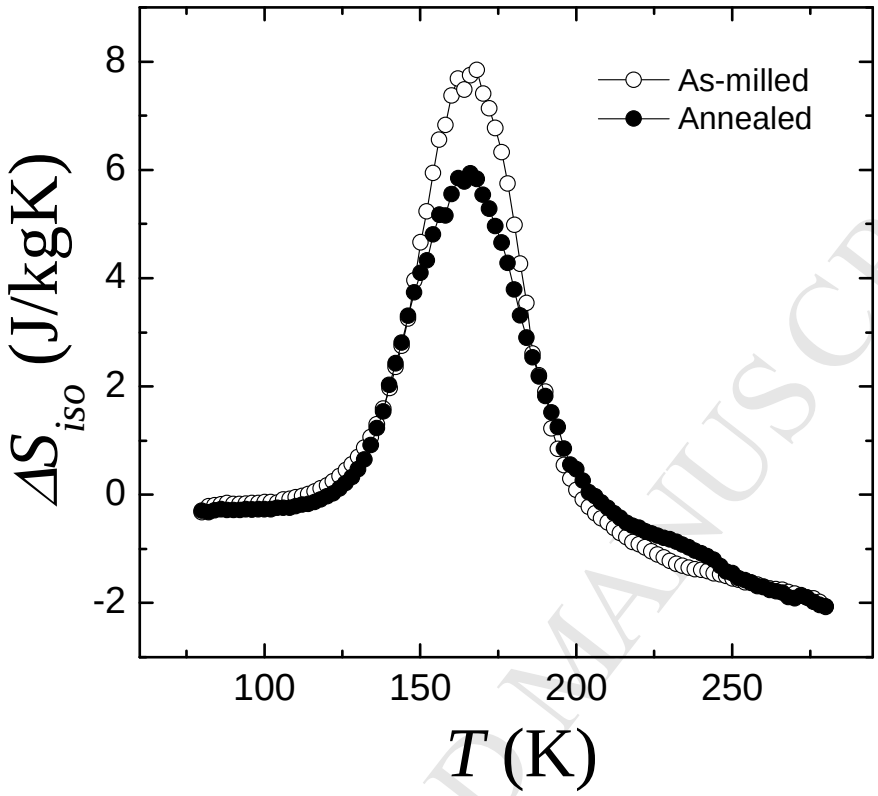

Fig.6

Sánchez-Alarcos et al.

Sample	T_M^{rev} *(100 Oe)* (K)	T_M^{rev} *(60 kOe)* (K)	T_C^a (K)	ΔM (Am^2/Kg)	ΔS (J/kgK)
As-milled	187	159	362	52	9.8
Annealed	188	159	360	40	8.1

Table 1

Sánchez-Alarcos et al.

State	Cubic $Fm\bar{3}m$ a = 5.9697 (0002)			Monoclinic $P2/m$ a=4.309(001) b=5.583(001) c=13.176(003) β=92.479(016)	
	Site	Atom	μ (μ_B)	Site	μ (μ_B)
As-milled	4*a*	0.94Mn+0.06Sn	3.11(2)	1*a*, 1*h*, 2*n*, 2*m*	2.47 (10)
	4*b*	0.47Mn+0.53Sn	1.14(2)	1*b*, 1*g*, 2*m'*, 2*n'*	-0.91(10)
	8*c*	0.88Ni+0.12Co	0.296*	2*j*, 2*k*, 4*o*, 4*o'*	0.296*
Annealed	4*a*	0.97Mn+0.03Sn	3.11(2)	1*a*, 1*h*, 2*n*, 2*m*	2.50(21)
	4*b*	0.49Mn+0.51Sn	1.19(2)	1*b*, 1*g*, 2*m'*, 2*n'*	-0.56(41)
	8*c*	0.90Ni+0.10Co	0.28*	2*j*, 2*k*, 4*o*, 4*o'*	0.28*

Atomic positions: 2*n*: x = 0.397(1), z = 0.201 (1); 2*m*: x = 0.032(1), z = 0.326 (1); 2*m'*: x = -0.034(4), z = 0.201 (1); 2*n'*: x = 0.453(5), z = 0.326 (1); 2*j*: y = 0.245(13); 2*k*: y = 0.221(7); 4*o*: z = 0.201 (1); 4*o'*: z = 0.326 (1)

Table 2

Sánchez-Alarcos et al.

Saturation magnetization increases in martensite but not in austenite after annealing

Local atomic disorder linked to defects hinders ferromagnetic coupling in martensite

Microstructural defects makes the magnetocaloric effect to be higher before annealing

Higher attainable magnetically-induced entropy change in the as-milled state

Stronger influence of induced defects on the vibrational entropy of the austenite